# Mechanisms of Electron-Induced Single Event Upsets in Medical and Experimental Linacs

Maris Tali, Rubén García Alía, Markus Brugger, Veronique Ferlet-Cavrois, Roberto Corsini, Wilfrid Farabolini, Arto Javainen, Maria Kastriotou, Heikki Kettunen, Giovanni Santin, Cesar Boatella Polo, Georgios Tsiligiannis, Salvatore Danzeca, and Ari Virtanen

***Abstract*—In this paper we perform an in-depth analysis of the single-event effects observed during testing at medical electron linacs and an experimental high-energy electron linac. For electron irradiations the medical linacs are most commonly used due to their availability and flexibility. Whereas previous efforts were made to characterize the cross-sections at higher energies, where the nuclear interaction cross-section is higher, the focus on this paper is on the complete overview of relevant electron energies. Irradiations at an electron linac were made with two different devices, with a large difference in feature size. The irradiations at an experimental linac were performed with varying energies and intensities to omit other possible effects.**

## I. Introduction

In modern space applications, the feature size of components has been steadily decreasing, driven by the ever-increasing need for larger storage and lower power. These new technologies have been shown to be sensitive to direct ionization from singly charged particles, including protons, muons and even electrons [1] [2] [3] as well as to being sensitive to indirect ionization events [4]. Moreover, similarly to traditional proton and neutron induced SEEs (Single Event Effect), electrons are also capable of causing these effects via electro-nuclear interactions [4].

Lately, increased interest has been shown for understanding the exact mechanisms behind these electron induced events and on understanding the results of these tests. The task is made more difficult by several factors which play an important role in low-energy electron irradiation campaigns. Due to the low probability of SEE caused by electrons, extra care has to be taken to unfold the various mechanisms which are involved in creating these SEEs. In this paper, the possible contribution from other particles created by the electron interactions with the beamline elements of the linac are analysed, while the possible prompt dose effects and elastic scattering mechanisms are discussed. The importance of eliminating these charge pile-up effects contribution possibility by conducting tests with varying dose rates is shown.

Date of original submission: 29.09.2017, date of revised submission: 10.04.2018, date of acceptance: 18.05.2018

M. Tali, R. G. Alía, M. Kastriotou, M. Brugger, R.Corsini, S. Danzeca , G. Tsiligiannis and W. Farabolini are with CERN, CH-1211 Geneve 23, Switzerland. (e-mail: maris.tali@cern.ch)

M. Tali, V. Ferlet-Cavrois, G. Santin, C. Boatella Polo and A. Zadeh are with the European Space Agency, ESTEC, 2200 AG Noordwijk, The Netherlands.

M. Tali, A. Javainen, H. Kettunen and A. Virtanen are with the Department of Physics, Accelerator Laboratory, University of Jyväskylä, FI-40014, Jyväskylä, Finland

We perform an in-depth analysis of the SEE observed during testing at medical electron linacs. For electron irradiations these type of accelerators are most commonly used due to their availability and flexibility. Whereas previous efforts were made to characterise the SEE mechanisms at higher energies, where the nuclear interaction cross section is larger [5], this paper takes a closer look at the electron energies starting from the threshold region. While [5] analysed in detail the electro- and photonuclear reactions which cause upsets in larger technologies, this paper aims to complement the in-depth analysis with further experimental results, including different technology sizes.

Irradiations at a medical linac at the RADEF facility at Jyvaskyla, Finland were made with two different devices, with large difference in feature size: the ESA SEU (single-event upset) monitor [6] [7] and an Artix-7 Field Programmable Gate Array (FPGA) test board. The tests were done with different energies and different fluxes. In previous work [4] similar irradiations have been presented, however in the present study additional possible explanations for the mechanisms involved are given. To evaluate the sensitivity of the Artix-7 device to potential direct ionization effects, a low-energy proton test was performed. The ESA SEU monitor is considered to be insensitive to direct ionization due to the large, $0.25\,\mu\mathrm{m}$ transistor size.

Additionally, tests with an experimental high-energy electron linac were performed at the VESPER facility at CERN, with energies ranging from $60\,\mathrm{MeV}$ up to $200\,\mathrm{MeV}$. The latter with the aim to give a more complete picture of the mechanisms governing the SEU at all energies relevant to the presented devices. As the Artix-7 displayed a higher cross-section, hypothesis for elastic electron/nucleon interactions as the main mechanism is presented, as suggested earlier by [8]. With all the relevant energies covered, a complete experimental electron-induced SEU Weibull fit could be found. This is relevant in light of the widespread use of commercial off-the-shelf (COTS) devices in demanding radiation environments. The irradiations at VESPER were performed with varying energies and intensities to rule out a potential prompt dose effect.

Additional tests were performed at VESPER with a slab of commonly used spacecraft shielding material, aluminium, placed in front of the detector. The goal was to evaluate the effect of secondary photons on the SEU cross-section of the ESA SEU monitor. In addition, a shielding material analysis was performed using FLUKA [9] [10]. The effect of the vari-

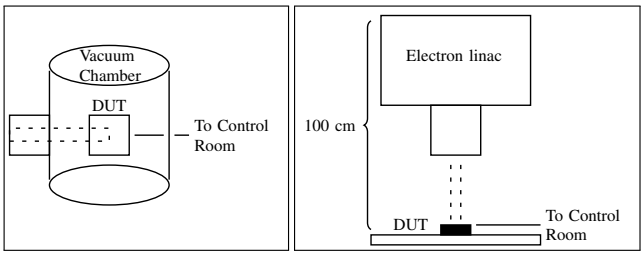


Fig. 1. Not to scale, left) Low-energy proton line test setup at RADEF right) Electron linac test setup, with the distance to the isocenter shown.

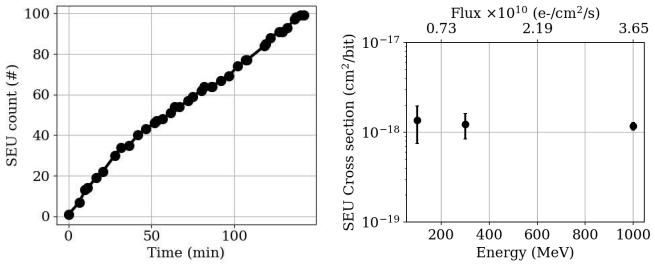


Fig. 2. Electron-induced SEUs in the ESA SEU monitor, left) upsets in time (dose rate $1\,\mathrm{krad(H_2O)/\,min}$, $20\,\mathrm{MeV}$) right) the cross section dependence on dose rate.

ous thicknesses of the materials on dose and flux of electrons, neutrons and photons was evaluated. The implications of the secondary particle creation on the ESA SEU monitor upset cross-section is evaluated and compared to the experimental measurements performed in VESPER.

Another motivation for a greater understanding in these electron-induced SEE are the planned missions to Jupiter. In the Jovian environment the greatest contribution to the overall dose level are the high-energy electrons in the trapped radiation belts [11]. The experimental electron-induced SEU Weibull fit was used to estimate the number of upsets in the ESA SEU monitor caused directly by the trapped electron spectra cited in [11].

## II. Facilities and Test Setups

### A. RADEF Facility

The RADEF (RADiation Effects Facility) consists of two caves. One contains the low- and high-energy proton and heavy ion lines and the other the electron linac [12]. The low-energy proton line can provide energies from about $500\,\mathrm{keV}$ to $6\,\mathrm{MeV}$. The maximum flux is dependent on the energy, at $1.5\,\mathrm{MeV}$ this corresponds to about $5 \times 10^7\,\mathrm{p/cm^2/s}$. The components under test are attached to a movable backplate in a vacuum chamber. The cables needed were connected through the vacuum feed-throughs to a computer at the control room as seen in Fig. 1 [13].

The electron linac at the RADEF facility, Varian 2100CD Clinac, is able to deliver electron beams with energies from $6\,\mathrm{MeV}$ up to $20\,\mathrm{MeV}$ and dose rates up to $1\,\mathrm{krad(H_2O)/min}$, which is a dose in water at the maximum calibration used in medical treatments. At the maximum dose rate the beam consists of $5\,\mu\mathrm{s}$ pulses with a period of $5\,\mathrm{ms}$. The typical beam size is $20\,\mathrm{cm} \times 20\,\mathrm{cm}$. For the irradiations a beam size of about $2\,\mathrm{cm} \times 2\,\mathrm{cm}$ was used. For the irradiations, the components are placed on a table located in the cave and connected to a computer in the control room through a $20\,\mathrm{m}$ Ethernet cable [14].

### B. RADEF Test Setup

The irradiations were performed on two devices, the ESA SEU monitor and the $28\,\mathrm{nm}$ Artix-7 FPGA test board Arty, both at nominal voltage. The ESA SEU monitor consists of 4 SRAMs, the technology node size is $250\,\mathrm{nm}$ [7].

The ESA SEU monitor was placed on the table at the isocenter, at $100\,\mathrm{cm}$ from the exit window of the linac, as shown on the right in Fig. 1. The irradiations were performed with a fixed dose rate and the number of upsets was noted at the end of each run. In order to investigate the possibility of prompt dose effects, as discussed in [4], the irradiations were performed with varying pulse charge to change the electron flux. The pulse charge was changed by reducing the current given by the electron source, the time structure of the pulses did not change. The cross section did not show any pulse charge dependence, as can be seen on the right in Fig. 2. As a result, the possibility that the upsets are caused by charge build-up can be ruled out.

The Artix-7 test board was placed on the test table, at $100\,\mathrm{cm}$ from the linac exit window. The FPGA package was opened before the test. The FPGA was programmed with a checkerboard pattern prior to irradiation and had a total of $1.44\,\mathrm{Mbit}$ of block RAM (BRAM). The BRAM was read periodically during testing through the UART interface of the FPGA, and the number of upsets was noted, no write or read operations were performed between the readouts on the BRAM.

### C. VESPER Facility

The VESPER facility, a part of the CLIC Test Facility CTF3 at CERN, is an electron linac, which provides a multi-purpose electron beam for accelerator technology tests. Since the recent upgrades to the beam-line and the possibility of running the facility using only one or two klystrons, the energy range of the facility is now improved and can reach from $60\,\mathrm{MeV}$ to $200\,\mathrm{MeV}$ [5].

### D. VESPER Test Setup

The ESA SEU monitor was placed in the beam to evaluate the electron-induced SEU cross section and confirm its energy dependence as described in [5]. To evaluate the beam spot evolution over time, a radio-sensitive film HD-V2 was used to precisely estimate the fluence of electrons covering each die of the ESA monitor and therefore more precisely evaluate the SEU cross-section. As the beam spot size is usually sufficient to cover all of the 4 dies uniformly, a more precise analysis was only necessary for the lowest energy runs. A run performed at VESPER demonstrating the uniformity of the beam shape and the stability of the beam charge over time can be seen in Fig. 3. The beam charge at the facility is monitored using a

beam charge monitor and the total fluence for the cross-section calculations is found using this detector.

The Artix-7 test board was placed on the test position, at the same position as the ESA SEU monitor. The FPGA package was opened before the test. The beam size was chosen so that it uniformly covered the FPGA die. The remaining test procedure was identical to the test procedure at RADEF.

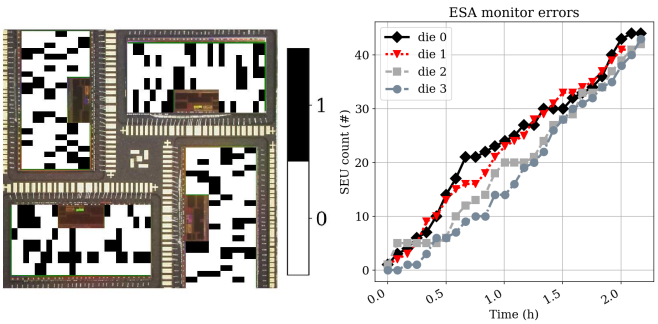


Fig. 3. left) Distribution of upsets in the ESA SEU monitor during a single run right) Evolution of upsets over time for the 4 die of the ESA SEU monitor.

## III. Experimental results

### A. RADEF ESA SEU monitor electron irradiation results

The ESA SEU monitor is programmed with a checkerboard pattern prior to irradiation and is then read out periodically, no read or write operations are performed between readouts. When an upset is found during the readout, the erronous bit is rewritten and added the seu count. The ESA SEU monitor was tested with 20 MeV, 16 MeV and 12 MeV electrons with varying electron fluxes. Due to the exceedingly low cross section, seeing an actual upset would require a high dose to the component, therefore at 12 MeV just an upper bound measurement was estimated. The test results are summarized in Table I. The cross section was calculated with the common definition:

$$\sigma = \frac{\#\ \text{SEUs}}{\phi \times \#\ \text{bits}} \tag{1}$$

where # SEUs is the number of SEU observed during the irradiation, # bits is the size of the memory array in bits and $\phi$ is the electron fluence in $\mathrm{e/cm^2}$. The ionization chambers in the linac give a dose measurement in terms of rad deposited in the maximum dose deposition depth in water. To estimate the number of electrons corresponding to a dose of 1 Gy, a FLUKA [9] [10] simulation was performed. In the simulation the energy deposited by a 20 MeV electron beam in a $1\,\mathrm{cm} \times 1\,\mathrm{cm} \times 0.1\,\mathrm{cm}$ block of air was scored, which gives us the LET in air. Although the dose of the accelerator was calibrated to water in the maximum dose depth, the LET in air is a close estimation of this value. The resulting calculated fluence to dose conversion factor is $3.65 \times 10^9\,\mathrm{e/cm^2/Gy}$.

### B. VESPER ESA SEU electron irradiation results

To evaluate the cross-section over the complete energy range for the ESA SEU monitor, tests at 60, 115 and 175 MeV were performed. The experimental cross-section from VESPER fits well with cross-sections measured both with the medical linac from RADEF and earlier measurements performed at VESPER in 2016 [5], with results ranging from 16 MeV up to 200 MeV. A summary figure can be seen in Fig. 4.

TABLE I
ESA SEU monitor electron irradiation results at the RADEF and VESPER linac, *an upper bound has been given for the 12 MeV irradiation. For the VESPER linac runs which have been gruped together for the Weibull fit are shown with brackets.

| **RADEF linac** | | | | |
|---|---|---|---|---|
| **Energy (MeV)** | **Dose rate (rad/min)** | **Total Dose (krad)** | **SEUs** | **Cross section ($\mathrm{cm^2}$/bit)** |
| 20.0 | $1.00 \times 10^3$ | 160 | 115 | $1.17 \times 10^{-18}$ |
| 20.0 | $3.00 \times 10^2$ | 13.3 | 10 | $1.14 \times 10^{-18}$ |
| 20.0 | $1.00 \times 10^2$ | 6 | 5 | $1.36 \times 10^{-18}$ |
| 16.0 | $1.00 \times 10^3$ | 60 | 2 | $5.44 \times 10^{-20}$ |
| 12.0 | $1.00 \times 10^3$ | 10 | 0 | $*1.63 \times 10^{-19}$ |
| **VESPER linac** | | | | |
| **Energy (MeV)** | **Duration(h)** | **Fluence (e-/$\mathrm{cm^2}$)** | **SEUs** | **Cross section ($\mathrm{cm^2}$/bit)** |
| **VESPER 2017** | | | | |
| 62 | 19.0 | $1.39 \times 10^{13}$ | 277 | $2.45 \times 10^{-18}$ |
| 60 | 58.0 | $1.79 \times 10^{14}$ | 2974 | $2.08 \times 10^{-18}$ |
| 115 | 17.0 | $1.39 \times 10^{13}$ | 374 | $3.33 \times 10^{-18}$ |
| 175 | 7.9 | $1.16 \times 10^{13}$ | 579 | $6.17 \times 10^{-18}$ |
| 175 | 11.8 | $1.72 \times 10^{13}$ | 653 | $4.67 \times 10^{-18}$ |
| **VESPER 2016** | | | | |
| 133 | 15.1 | $3.95 \times 10^{12}$ | 81 | $1.87 \times 10^{-18}$ |
| 133 | 14.8 | $4.20 \times 10^{12}$ | 141 | $3.42 \times 10^{-18}$ |
| 170 | 8.1 | $3.01 \times 10^{12}$ | 143 | $4.29 \times 10^{-18}$ |
| 170 | 13.9 | $5.09 \times 10^{12}$ | 169 | $2.88 \times 10^{-18}$ |
| 206 | 16.0 | $2.60 \times 10^{13}$ | 1558 | $5.97 \times 10^{-18}$ |
| 206 | 7.5 | $5.30 \times 10^{12}$ | 283 | $5.09 \times 10^{-18}$ |
| 206 | 16.0 | $1.04 \times 10^{13}$ | 545 | $4.68 \times 10^{-18}$ |

### C. Experimental Weibull fit for electron-induced SEU in the ESA SEU monitor

Since electron measurements have now been performed over a wide energy range, a total electron-induced SEU cross-section Weibull fit could be found, as seen in Fig. 4. The parameters for the Weibull fit were as follows: XSsat = $3.84 \times 10^{-18}\ \mathrm{cm^2/bit}$, Lo = 16.0 MeV, W = 45.3 MeV and s = 0.62. The main difference between the simulated electron-induced SEU cross-section and the one reported in [5] is the width parameter W. The main reason for the difference is the fact that the Weibull fits were found separately for electrons and photons. As discussed in this paper, since the photons play an important role in the total SEU cross-section, the real response of devices to electron irradiation will be a combined contribution from electrons and photons. Therefore, to more accurately evaluate the electron-induced upset cross-section, an analysis of possible contributions of secondary particles should be performed.

To further estimate the secondary particle contribution, FLUKA simulations with various common spacecraft shielding materials placed in front of the ESA SEU monitor are

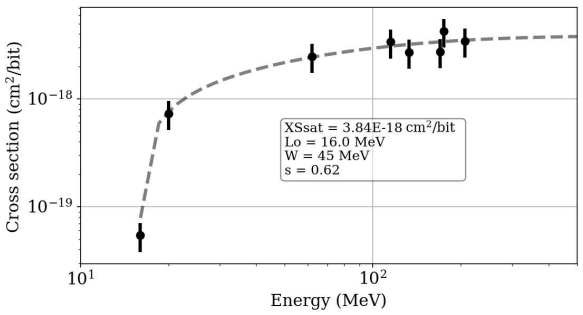


Fig. 4. The Weibull fit for electron induced SEU for the ESA SEU monitor based on measurements from the VESPER and the RADEF facility.

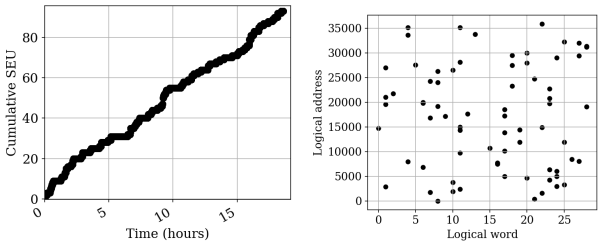


Fig. 5. left) Cumulative SEU of Artix-7 60 MeV run at VESPER right) Logical map of SEU of Artix-7 60 MeV run at VESPER.

described in section IV-D. To verify the FLUKA simulations, a measurement was performed in the VESPER facility with a slab of $1\,\mathrm{cm}$ of aluminium placed directly in front of the device. The resulting cross-section at $175\,\mathrm{MeV}$ was $3.26 \times 10^{-17}\ \mathrm{cm}^2/\mathrm{bit}$, compared to $5.26 \times 10^{-18}\ \mathrm{cm}^2/\mathrm{bit}$ without the aluminium slab, or about 6 times higher. This measurement result confirms the theory that secondary photons contribute to the upsets seen in electron beam irradiation. To rule out that the higher overall flux caused by the secondary particles created by the aluminium slab was causing a prompt dose effect, measurements with two different intensities were performed. For a beam charge of $9\,\mathrm{pC}$ a cross-section of $3.216 \times 10^{-17}\ \mathrm{cm}^2/\mathrm{bit}$ was seen. At $2\,\mathrm{pC}$ the cross-section was $3.068 \times 10^{-17}$, the difference being 5% and therefore statistically comparable. As shown by [1], if the upsets were indeed caused by prompt dose effects, the cross-section would vary linearly with the intensity. Since the cross-section does not vary with the varying intensity, we can conclude that the upsets were caused by electro- and photo-nuclear interactions, as described in [5].

### *D. VESPER and RADEF Artix-7 electron irradiation results*

Two irradiation runs were made with varying dose rate. Only 2 upsets in the memory array were observed during the irradiations. For a total deposited dose of $100\,\mathrm{krad}$, this corresponds to a cross section of $3.81 \times 10^{-19}\,\mathrm{cm}^2/\mathrm{bit}$ at $20\,\mathrm{MeV}$.

The Artix-7 was irradiated at the 2 extreme energies at VESPER, $60\,\mathrm{MeV}$ and $201\,\mathrm{MeV}$. The resulting cross-sections are $2.01 \times 10^{-17}\,\mathrm{cm}^2/\mathrm{bit}$ and $4.76 \times 10^{-17}\,\mathrm{cm}^2/\mathrm{bit}$ respectively. An example of one of the $60\,\mathrm{MeV}$ runs can be seen in Fig. 5, which shows the linearity of the runs. An example of the distribution of the logical addresses can be seen in Fig. 5. Although the physical mapping of the BRAM is not available, a map of the logical addresses of the memory provides a first proof that these upsets are random, and not clustered or periodically occurring. A summary of both runs can be seen in Table II.

### *E. Experimental Weibull fit for electron-induced SEU in the Artix-7 BRAM*

The experimental Weibull fit for the electron-induced SEU for the Artix-7 can be seen in Fig. 6. The parameters of the fit are as follows : XSsat = $5 \times 10^{-17}\ \mathrm{cm}^2/\mathrm{bit}$, Lo = $19.9\,\mathrm{MeV}$, W = $100\,\mathrm{MeV}$ and s = 0.6. The first, and most important difference with the ESA monitor response is the absolute value of the saturation cross-section, the Artix-7 being 1 order of magnitude higher. According to the hypothesis that the photo- and electro-nuclear interactions cause these single event upsets, which holds for a device with a high critical charge like the ESA SEU monitor, as described in [5], the cross-section would have to be lower for smaller sensitive volume sizes. As the cross-section is clearly higher, an additional effect has to be contributing to the error generation. There have been several hypothesis into competing effects, such as elastic electron/nucleon interactions described in [8]. To get a first estimation of the cross-section of a more modern technology, such as the Artix-7, for photo- and electro-nuclear reaction induced SEU, an amalgamation of a physical RPP simulation and a complete nuclear physical simulation was used to estimate the critical charge for the device. First, energy deposition simulations for electrons and protons were made for the $0.3\,\mu\mathrm{m} \times 0.3\,\mu\mathrm{m}$ side sensitive volume geometry. Then, the experimental saturated SEU cross-section for protons for the same device, found in [15] to be $9 \times 10^{-15}\,\mathrm{cm}^2/\mathrm{bit}$ was used. To estimate the critical charge for the Artix-7, the deposited energy at this saturation cross-section is used, and is found to be $3.7\,\mathrm{fC}$. Then, the electron simulation, seen on the left in Fig. 9, is used to estimate the photo- and electro-nuclear interaction cross-section at $3.7\,\mathrm{fC}$ of deposited charge and is shown to be $4 \times 10^{-18}\,\mathrm{cm}^2/\mathrm{bit}$ at $200\,\mathrm{MeV}$ and $7 \times 10^{-20}\,\mathrm{cm}^2/\mathrm{bit}$ at $20\,\mathrm{MeV}$.

Previous tests of the Artix-7 device for $20\,\mathrm{MeV}$ give the cross section to be in the order of a couple $10^{-18}\ \mathrm{cm}^2/\mathrm{bit}$ [4]. The hypothesis given was electro- and photo-nuclear effects. The difference between the value obtained in this work and [4] can be explained by the large uncertainties in cross-section in the threshold region, and therefore are still compatible. However, at higher energies, the cross-section is clearly too large to be explained purely by the electro- and photo-nuclear events. It is feasible that a combination of the two effects, electro- and photo-nuclear and elastic electron/nucleon interactions, can explain the higher cross-section values at higher energies. Further studies are needed in order to more precisely simulate the effects and to understand for which technology nodes and critical charge values the effects are dominating.

As introduced in [16], the maximum energy an elastic electron silicon recoil can transfer displays a very strong

energy dependence on the initial electron energy. A 10 MeV electron deposits maximally about 10 keV whereas a 20 MeV electron deposits about 30 keV. Since the SEU cross-section displays a very strong energy dependence, it is conceivable that the critical energy lies somewhere between the 10 keV and 30 keV, which would explain this dependence.

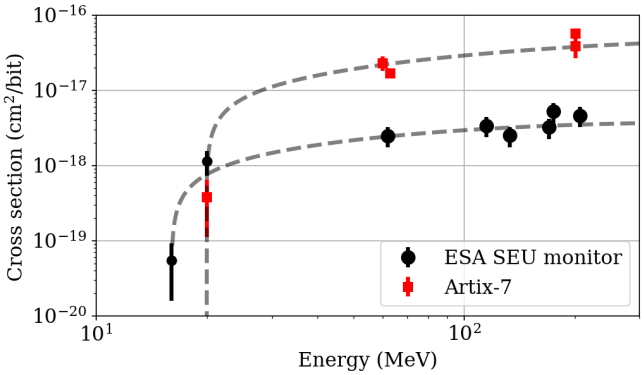


Fig. 6. The Weibull fit for electron induced SEU for the Artix-7 based on measurements from the VESPER and the RADEF facility.

### F. RADEF Artix-7 low-energy proton irradiation results

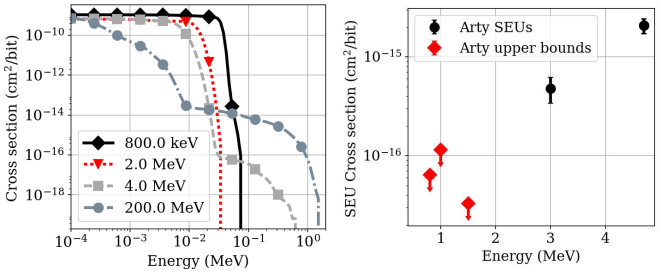


Fig. 7. left) FLUKA simulation for the 300 nm × 300 nm sensitive volume geometry and right) results of the low-energy proton irradiation of the Artix-7 board.

To investigate the possibility of direct ionization contributing to the SEUs, irradiations were done at a low-energy proton line at RADEF. The physical process through which electrons and protons cause upsets in this energy region are the same, with the maximum LET value for electrons being lower. Therefore, an irradiation with protons was selected. The tests were performed in vacuum, and the test procedure was identical to the electron linac tests performed with the same component.

The Artix-7 test board recorded no upsets below 3 MeV. For the lower energies, the upper-bound cross section has been estimated. The results are summarized in Table II and illustrated on the right of Fig. 7. It was observed that this device is not sensitive to direct ionization from protons, therefore, it can be concluded that the same holds true for electrons. FLUKA energy deposition simulations, which are described in more detail in section IV-B, were run and their results can be seen in Fig. 7. The cross-section as a function

TABLE II
ARTIX-7 IRRADIATION RESULTS AT THE LOW ENERGY PROTON AND ELECTRON LINES AT RADEF AND THE VESPER FACILITY. FIELDS MARKED WITH * ARE THE UPPER BOUNDS FOR THE CROSS SECTIONS

| **RADEF Low Energy Proton** | | | | |
|---|---|---|---|---|
| **Energy (MeV)** | **Flux (p/cm²/s)** | **Fluence (p/cm²)** | **SEUs** | **Cross section (cm²/bit)** |
| 4.7 | $5 \times 10^7$ | $1.21 \times 10^{10}$ | 36 | $2.07 \times 10^{-15}$ |
| 4.7 | $1 \times 10^7$ | $1.04 \times 10^{10}$ | 31 | $2.07 \times 10^{-15}$ |
| 3.0 | $6 \times 10^7$ | $1.74 \times 10^{10}$ | 12 | $4.79 \times 10^{-16}$ |
| 1.5 | $5 \times 10^7$ | $2.12 \times 10^{10}$ | 0 | $*3.27 \times 10^{-17}$ |
| 1 | $5 \times 10^6$ | $6.08 \times 10^9$ | 0 | $*1.14 \times 10^{-16}$ |
| 0.8 | $1 \times 10^7$ | $1.09 \times 10^{10}$ | 0 | $*6.37 \times 10^{-17}$ |
| **RADEF Electron** | | | | |
| **Energy (MeV)** | **Dose rate (rad/min)** | **Total Dose (krad)** | **SEUs** | **Cross section (cm²/bit)** |
| 20.0 | $1.00 \times 10^2$ | 100 | 2 | $3.81 \times 10^{-19}$ |
| **VESPER** | | | | |
| **Energy (MeV)** | **Duration(h)** | **Fluence (e-/cm²)** | **SEUs** | **Cross section (cm²/bit)** |
| 60 | 3.1 | $6.30 \times 10^{11}$ | 21 | $2.37 \times 10^{-17}$ |
| 63 | 18.6 | $3.80 \times 10^{12}$ | 93 | $1.70 \times 10^{-17}$ |
| 201 | 1.8 | $1.98 \times 10^{11}$ | 11 | $3.86 \times 10^{-17}$ |
| 201 | 4.3 | $4.66 \times 10^{11}$ | 38 | $4.76 \times 10^{-17}$ |

of critical energy is constant in the direct ionization region and then sharply falls off. The following peak in energy deposition comes from nuclear or indirect ionization events. As can be seen, for energies below about 3 MeV, almost no energy is deposited through indirect ionization, which supports the experimental results.

## IV. Analysis of the Electron Induced SEU Mechanisms

### A. Analysis of the Electron Beam at the RADEF Linac

The dose rate of the RADEF linac is monitored by an ionization chamber. The linac has been characterized extensively, and precise dose depth measurements have been performed using PTW 30013 and PTW 34001 ionization chamber and a water phantom.

For the purpose of understanding precisely the upsets caused by the beam, the composition and spectrum of the beam particles was analysed in a FLUKA simulation. A first iteration of the linac geometry, which includes the main components interacting with the beam has been created. These are the 4 mm beryllium beam exit window, the 2.5 mm aluminium diffusion foil spreading the pencil beam from the accelerator and the two sets of 2.5 cm lead collimators to control the beam size.

For the 20 MeV beam, the exact electron beam kinetic energy is 22.3 MeV [17]. As a first approximation, the accuracy of the FLUKA simulation was assessed by comparing it with the dose depth curves obtained with the beam calibration measurements. The results are deemed suitable for this first analysis, and show a maximum discrepancy of about 15% up to a dose depth of 9 cm, as can be seen on the left of Fig. 8. The beam spectra were also simulated in order to estimate the contribution to the cross section of the relevant

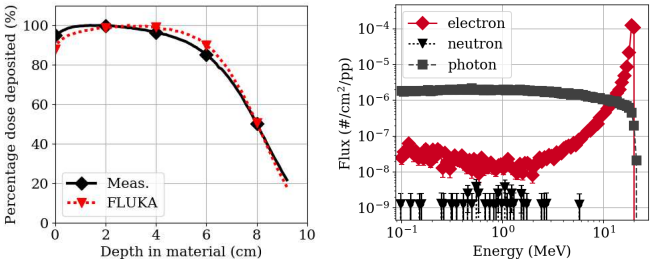


Fig. 8. left) Comparison of the FLUKA simulation and experimental measurements at the electron linac of 20 MeV electrons in water right) Flux of electrons, neutrons and photons scored at the surface of the water target in the clinac FLUKA simulation, logarithmic binning is used.

particles: electrons, photons and neutrons. Due to the electron beam interacting with various elements of the linac, there is a sizable flux of mostly bremsstrahlung photons generated by the electron-matter interactions.

### B. FLUKA Energy Deposition Simulation

To estimate the energy deposited by 20 MeV electrons in the ESA SEU monitor, with a feature size of 0.25 µm and the Artix-7, with a feature size of 28 nm, two geometries were created. Both geometries consist of a stack of aluminium and silicon dioxide layers, with the bottom layer representing the active silicon, also containing cubes of sensitive volumes for energy deposition scoring. The geometry representative of the ESA SEU monitor had a sensitive volume side of 3 µm × 3 µm, which has been shown earlier to match well with experimental data [5]. Since no heavy-ion irradiation was performed for the Artix-7, an estimation for a more modern technology size SV was used. A side of 300 nm × 300 nm is a good estimation for a smaller features size, as described for a 45 nm technology in [4] where the procedure described in [18] was implemented. For both a sensitive volume depth of 0.5 µm was used.

The simulation results for electrons can be seen in Fig. 9.

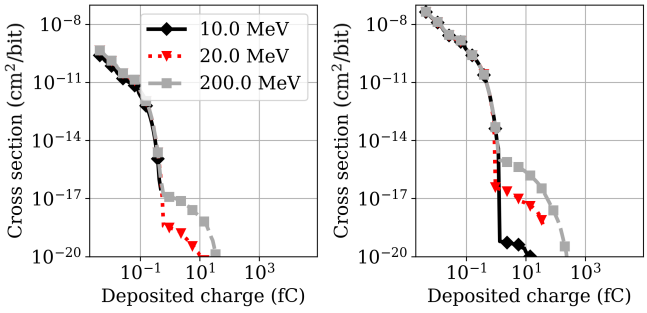


Fig. 9. FLUKA energy deposition simulations for the left) 0.3 µm × 0.3 µm and right) 3 µm × 3 µm sensitive volume geometries.

### C. Contribution of Photons to the Cross Section

As observed from the first estimation of the fluxes of the particles created by the electron beam interaction with the linac elements in Fig. 8, in addition to electrons, photons with energies up to the beam energy are created. These photons have a higher probability of causing an upset at the same energy than an electron due to the higher nuclear interaction cross section. Because of this, the photon contribution to the SEU cross section is comparable to that of the 20 MeV electrons. To estimate the contribution of photons to the cross section, the simulated particle fluxes are folded with the Weibull responses for each particle, which were estimated in [5]. The folding of the simulated fluxes and the Weibull function is described as:

$$N_i/pp = \int \frac{d\phi_i(E)/pp}{dE} \cdot \sigma_i(E)\, dE \tag{2}$$

where $N_i$ is the expected number of upsets per primary particle from FLUKA, $\frac{d\phi_i(E)/pp}{dE}$ is the flux per primary particle in $\#/\mathrm{MeV/pp}$ and $\sigma_i(E)$ is the Weibull estimated cross section for the given particle.

Finally, to obtain the estimated cross section $\sigma_{calc}$, the result $N_i/pp$ has to be normalized to the total integrated flux of electrons per primary particle $\phi/pp$, which primarily contribute to the dose. The flux per primary particle can be seen in Fig. 4, and is obtained from the FLUKA simulation of the electron linac. Therefore:

$$\sigma_{calc} = \frac{N_i/pp}{\int \phi(E)/pp\, dE} \tag{3}$$

For the ESA SEU monitor, the folding at 20 MeV, the contribution from electrons, $1.69 \times 10^{-19}\,\mathrm{cm^2/bit}$, and photons, $2.47 \times 10^{-19}\,\mathrm{cm^2/bit}$, is comparable. At 16 MeV, the Weibull fit threshold was estimated as 15.9 MeV [5], therefore only the photons contribute to the cross section, which is $6.56 \times 10^{-21}\,\mathrm{cm^2/bit}$. The neutron contribution at both energies was negligible.

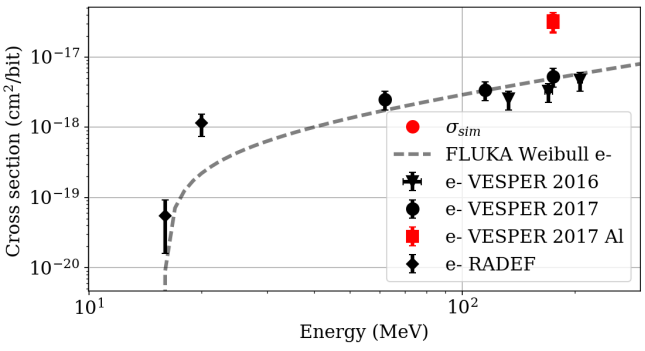


Fig. 10. The FLUKA based Weibull fit for electron induced SEU for the ESA SEU monitor [5] and the measurements from the VESPER and the RADEF facility, including a measurement with an aluminium slab, sum of $\sigma_{sim}$ from (3) for each energy, from folding the Weibull fit and the simulated spectra, seen in Fig. 8.

### D. Shielding Material Analysis

Due to the observation that photons have a large impact on the cross-section, a further study of this effect has been conducted. In space missions, it is imperative to protect the sensitive electronics inside the spacecraft from the harmful

effects of radiation. Often the shielding consists of several layers of material, and the general strategy is to place a thin layer of dense material, for example tantalum or lead in the outer layer and then a thicker layer of lower-density material, like aluminium on the inner layers. The combined effect is then that the high density material generates secondary particles and the thicker layer of material dampens the generated spectra of various particles. Although this strategy works well for dose, the amount of secondary photons generated presents a challenge. The effect of various thicknesses of shielding materials is then analysed. Whereas the impact of secondaries created in shielding in electron-dominated environments were studied in [19] and [20] in the context of displacement damage, this work focuses on single-event upsets.

Firstly, the materials chosen are commonly used in spacecraft shielding: aluminium, lead, tantalum and a final material chosen was copper for direct comparison with earlier experimental data from [5]. The material thicknesses were chosen from 1 to 40 mm, which are the typical thicknesses of shielding used. A 200 MeV electron beam impinged on the various thicknesses of the shielding material and the resulting secondary particle spectra and deposited dose in air were scored. The resulting particle spectra for aluminium and tantalum can be seen in Fig. 11. The denser material tantalum generates a much larger amount of secondaries, especially neutrons.

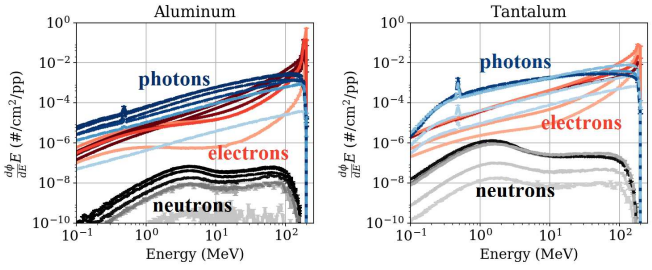


Fig. 11. Spectra of secondary particles generated by left) aluminium right) tantalum. Lighter color means thinner shielding, darker color means thicker shielding.

To estimate the contributions that the various particles have on the SEU cross-section for the ESA SEU monitor the flux of particles exceeding 10 MeV was found and can be seen in Fig. 12. The most obvious effect that the shielding has on the neutron and photon flux is that of increasing it by several orders of magnitude even after relatively small shielding thicknesses. As expected, the denser materials tantalum and lead produce more secondaries and the particle fluxes are therefore higher than for the less dense aluminium. However, the electron fluxes remain relatively constant regardless of shielding material and thickness. This is a good indication that the additional shielding will increase the SEU contribution for neutrons and photons, whereas the electron cross-section will remain relatively constant. It is worth noting that the neutron cross section is about 5 orders of magnitude lower than the electron cross-section. However, since the SEU cross-section of neutrons is much higher than that of the electrons and photons, the contribution has been further analysed.

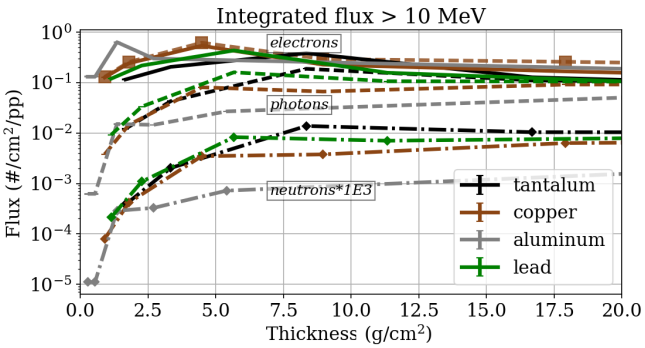


Fig. 12. Integrated flux over 10 MeV, these are the particles which mainly contribute to the SEU cross-section for the ESA SEU monitor.

To analyze the contributions of different particles to the SEU cross section of the ESA SEU monitor, the various particle spectra were folded with the corresponding Weibull response for each particle, described in [5], of the monitor and the results can be seen in Fig. 13. As expected, the contribution of photons to the cross-section is dominant after even thin shielding thicknesses, the increase of the cross section for aluminium is about two orders of magnitude for photons. Since aluminium is a commonly used shielding material, the analysis clearly demonstrates the challenges this radiation environment poses for even a relatively old technology. Even though the SEU cross-section for electrons is relatively constant, the real effect of the high-energy electrons is due to the secondary photons produced by Bremsstrahlung as these electrons travel through the shielding materials.

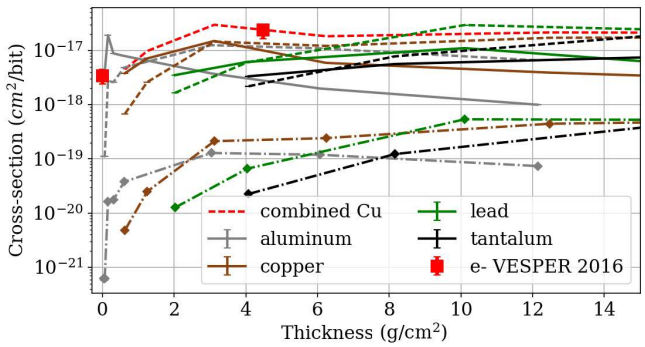


Fig. 13. SEU cross-section contribution for secondary protons, neutrons and photons produced by a 200 MeV electron beam transported through common shielding materials for the ESA SEU monitor. The line shows the electrons, the dashed line are the photons and the dashed and dotted line are the neutrons.

### *E. Analysis of Elastic Recoils Contribution to the cross section*

In order for an elastic recoil to cause an upset, it has to deposit a higher charge than the critical charge limit for a given device. For the ESA SEU monitor the critical charge is considered to be about 10 fC. As discussed in [8], the maximum charge an elastic recoil can deposit at 20 MeV is about 0.5 fC. Therefore, it is impossible that an upset caused by an elastic interaction recoil takes place in our device

[12] A. Virtanen, "Radiation effects facility RADEF," in *Proceedings of the Eighth IEEE International On-Line Testing Workshop (IOLTW 2002)*. IEEE, 2002, p. 188.

[13] H. Kettunen, V. Ferlet-Cavrois, P. Roche, M. Rossi, A. Bosser, G. Gasiot, F.-X. Guerre, J. Jaatinen, A. Javanainen, and F. Lochon, "Low energy protons at RADEF-application to advanced eSRAMs," in *Radiation Effects Data Workshop (REDW), DOI: 10.1109/REDW.2014.7004577*. IEEE, 2014, pp. 147–150.

[14] "RADiation Effects Facility RADEF - Linear electron accelerator," 2016. [Online]. Available: https://www.jyu.fi/fysiikka/en/research/accelerator/radef/facility/linac

[15] F. S. G. Tsiligiannis, S. Danzeca, R. Garcia-Alia, A. Infantino, A. Lesea, M. Brugger, A. Masi, S. Gilardoni, "Radiation Effects on Deep Submicron SRAM-based FPGAs for CERN applications," *IEEE Trans. Nucl. Sci. (submitted)*, vol. NA, 2017.

[16] A. Akkerman, J. Barak, and N. M. Yitzhak, "Role of Elastic Scattering of Protons, Muons, and Electrons in Inducing Single-Event Upsets," *IEEE Trans. Nucl. Sci.*, vol. 64, no. 10, pp. 2648–2660, Aug. 2017.

[17] J. C. Liu, K. R. Kase, X. S. Mao, W. R. Nelson, J. H. Kleck, and S. Johnson, "Calculations of Photoneutrons from Varian Clinac Accelerators and Their Transmissions in Materials," in *Slac-Pub-7404*, no. SLAC-PUB-7404, Nov. 1997, pp. 1–5. [Online]. Available: http://www.slac.stanford.edu/cgi-wrap/getdoc/slac-pub-7404.pdf

[18] R. A. Weller, M. H. Mendenhall, R. A. Reed, R. D. Schrimpf, K. M. Warren, B. D. Sierawski, and L. W. Massengill, "Monte Carlo simulation of single event effects," vol. 57, no. 4, pp. 1726–1746, Aug. 2010.

[19] C. Dale, P. Marshall, B. Cummings, L. Shamey, and A. Holland, "Displacement Damage Effects in Mixed Particle Environments for Shielded Spacecraft CCDs," *IEEE Trans. Nucl. Sci.*, vol. 40, no. 6, pp. 1628–1637, Dec. 1993.

[20] L. Alexander, S. Allen, and N. L. Bindoff, "Spacecraft displacement damage dose calculations for shielded CCDs," *High-Resolution Sensors and Hybrid Systems*, vol. 1656, pp. 476–487, Aug. 1992.